Late Pleistocene climate conditions in the north Chilean Andes drawn from a climate–glacier model

Christoph Kull,[1] Martin Grosjean[2]
[1]*Geographical Institute, University of Berne, CH-3012 Berne, Switzerland*
[2]*Swiss Federal Institute for Snow and Avalanche Research, CH-7260 Davos, Switzerland*

ABSTRACT. A climate–glacier model was used to reconstruct Late-glacial climate conditions from two case-study glaciers at 18° and 22° S in the arid (sub)tropical western Andes of northern Chile. The model uses (i) the geometry of the Late-glacial maximum glaciation, (ii) modern diurnal and annual cycles, amplitudes and lapse rates of the climate, (iii) empirical–statistical sublimation, melt and accumulation models developed for this area, and (iv) dynamic ice flow through two known cross-sections for steady-state conditions. The model is validated with modern conditions and compares favorably with the glaciological features of today. The mass-balance model calculates the modern equilibrium-line altitude at 18° S as high as 5850 m (field data 5800 m), whereas no glaciers exist in the fully arid southern area at 22° S despite altitudes above 6000 m and continuous permafrost. For Late-glacial times, the model results suggest a substantial increase in tropical summer precipitation ($\Delta P = +840$ $(-50/+10)$ mm a^{-1} for the northern test area; +1000 $(-10/+30)$ mm a^{-1} for the southern test area) and a moderate temperature depression ($\Delta T = -4.4$ $(-0.1/+0.2)$ °C at 18° S; −3.2 (± 0.1) °C at 22° S). Extratropical frontal winter precipitation (June–September) was <15% of the total annual precipitation. A scenario with higher winter precipitation from the westerlies circulation belt does not yield a numerical solution which matches the observed geometry of the glaciers. Therefore, we conclude that an equatorward displacement of the westerlies must be discarded as a possible explanation for the late Pleistocene glaciation in the Andes of northern Chile.

1. INTRODUCTION

The arid central Andes have become a key site for the study of abrupt, high-amplitude climatic changes during late Pleistocene and Holocene times. Ice cores (Thompson and others, 1995, 1998), paleolake sediments (e.g. Grosjean and others, 1995; Sylvestre and others, 1999) and glacial deposits (Messerli and others, 1996; Clayton and Clapperton, 1997) provide evidence of dramatic changes in the effective moisture regime (precipitation minus evaporation). However, major uncertainties exist with regard to the quantitative assessment of temperature and/or precipitation changes, potential changes in seasonality and the origin of the moisture supply (extratropical winter rainfall vs tropical summer rainfall). Based on depressions of the Late-glacial equilibrium-line altitudes (ELAs), Seltzer (1992, 1993) estimated a reduction of the mean annual temperature $\Delta T = -3.5 \pm 1.6$°C for the Bolivian Andes. Clayton and Clapperton (1997) calculated an increase in annual precipitation rates of +600 mm and a temperature reduction of 2.7 ± 0.9°C for Late-glacial glaciers in the Uyuni basin (20° S). Moreover, water-balance models of the Late-glacial paleolake Tauca suggest substantial increases in summer precipitation in the order of 300 mm (Hastenrath and Kutzbach, 1985), and 315 ± 45 mm at a temperature reduction of 3°C (Kessler, 1985) for the Peruvian–Bolivian Altiplano. Grosjean (1994) estimated precipitation rates of >500 mm (increase of 300 mm) for Late-glacial paleolakes in the more arid areas in Chile adjacent to the south at 23° S. The origin of the Late-glacial moisture remains a matter of debate. Kessler (1991), Markgraf (1993) and Grosjean and others (1995) favor tropical summer precipitation, whereas Servant and others (1993) make a case for strengthened westerly winter precipitation. This controversy is a key issue when evaluating past changes in atmospheric circulation belts.

The aim of this paper is to reconstruct quantitatively climatic conditions which were suitable to sustain the field-surveyed late Pleistocene glaciers at steady-state conditions. Results of a climate–glacier model (Kull, 1999) suggest for a first case-study area in the fully arid Andes at 22° S that modern climate–mass-balance relationships and ice-flow dynamics provide numerical solutions which effectively reflect the geometry of the mapped Pleistocene glaciers in this area. Here we compare modeling results from two different test areas along a north–south precipitation gradient from the fully arid Andes at 22° S to the area with dominant tropical summer precipitation at 18° S. We also test different seasonal precipitation scenarios (with winter and/or summer precipitation), and show that a scenario with exclusively increased winter precipitation does not yield a numerical solution which matches the geometry of the Pleistocene case-study glaciers.

2. RESEARCH AREA AND MODERN CLIMATE

The research area is located between 18° and 23° S in the western Altiplano of northern Chile near the border with Bolivia (Fig. 1). Today, precipitation falls mainly as tropical summer rains, due to a southward shift of the intertropical convergence zone which results in a strong precipitation

https://doi.org/10.3189/172756500781832611 Published online by Cambridge University Press

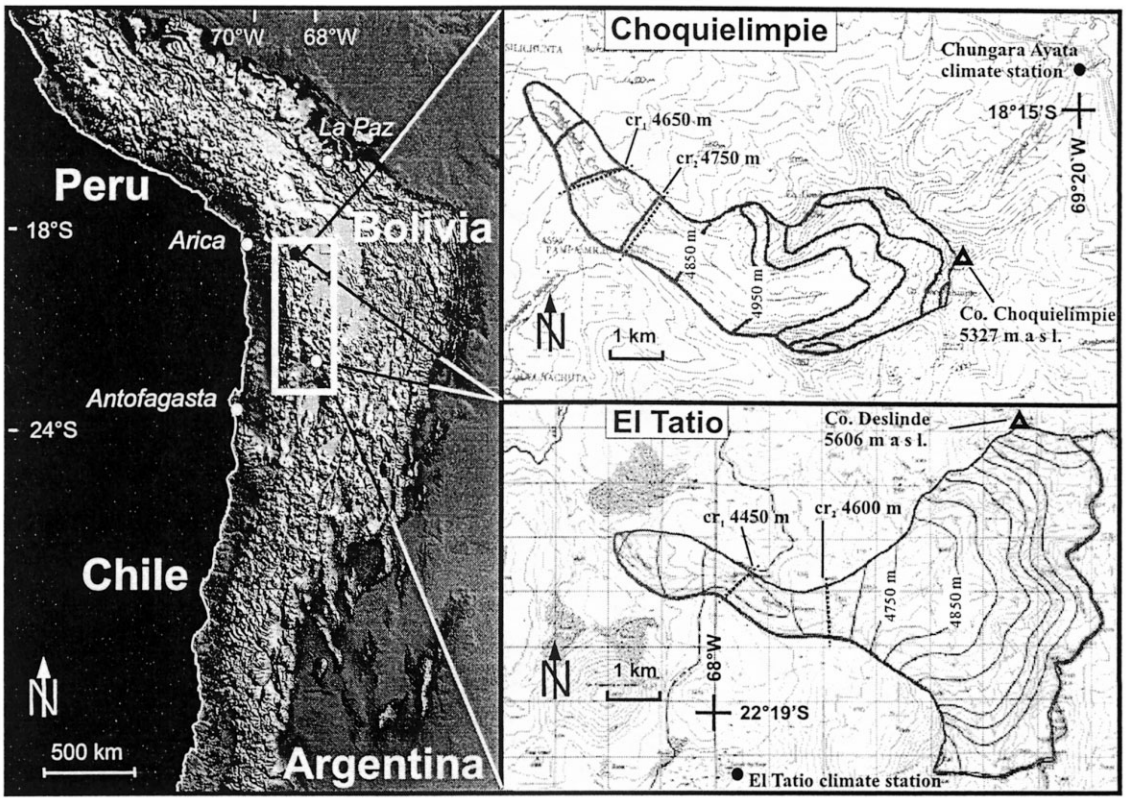

Fig. 1. Map showing the two case-study glaciers on Cerro Choquielimpie (18° 17′ S, 69° 12′ W; 5327 m a.s.l.) and on Cerro Deslinde–El Tatio (22° 15′ S, 68° W; 5606 m a.s.l.) in the western central Andes of the Altiplano, northern Chile. Both glaciers are located on west-facing slopes in east–west orientation. The solid lines represent the reconstructed ice isohypses (100 m interval); the dotted lines are the cross-sections cr_1 and cr_2 used in the model.

gradient from 450 mm a^{-1} in the north at 18° S to <250 mm a^{-1} in the southern test area at 22° S. High diurnal temperature changes of up to 16°C are characteristic for the daily temperatures; monthly mean temperatures vary in the order of 7°C during the year. The mean annual temperature is 3.6°C at 4300 m a.s.l. (Table 1).

Due to the lack of moisture, there is now an absence of perennial snowfields and glaciers in the area south of 19° S even in the continuous permafrost belt above 5600 m. This phenomenon is known as "thermal readiness" (Messerli, 1973; Grosjean and others, 1998), and shows that ablation rates (sublimation and melt) greatly exceed accumulation rates in all geo-ecological altitudinal belts. The modern ELA of the southernmost glacier in the summer precipitation belt of the western Andes at 18° S is found at approximately 5800 m (Cerro Guaillatiri 6046 m; Jenny and Kammer, 1996). Further south, a modern ELA no longer exists, and peaks well above 6000 m are free of glaciers.

However, late Pleistocene glaciation was very lively in the entire research area 18–22° S, where late Pleistocene ELAs were depressed to approximately 4600–4900 m (Jenny and Kammer, 1996; Klein and others, 1999). We selected two case-study areas (Fig. 1): the massifs of Cerro Choquielimpie (18° 17′ S, 69° 12′ W; 5327 m a.s.l.) and El Tatio (22° 15′ S, 68° W; 5606 m a.s.l.) which feature surprising Pleistocene valley glaciers up to 12 km long and provide a suitable topographical setting for modeling.

3. RECONSTRUCTION OF THE GLACIER BED AND CLIMATE DATA FOR THE MODEL

Ice isohypses in the former accumulation areas are estimated from the basal shear stress ($\tau = 100$ kPa) along the central flowlines, and are interpolated with a contour interval of 100 m. The ice isohypses are used only to reconstruct the area elevation distribution of the former glaciers. Within the area of the former glacier tongues (ablation area), ice isohypses are determined by the heights of the lateral moraines. Due to the well-defined geometry, cross-sectional areas of the former glaciers can be measured with a high degree of confidence, thus allowing reliable calculation of the mass flux at the cross-sections. Trapezoidal cross-sections were reconstructed at two different altitudes (Choquielimpie at 4650 and 4750 m, El Tatio at 4450 and 4600 m; Fig. 1). The glacier beds show a uniform gentle slope of 2.5° (Choquielimpie) and 5° (El Tatio) and a uniform west–east aspect. At El Tatio, glacial striations are found at altitudes up to 5300 m, indicating that the Pleistocene glaciers were temperate. First direct datings of striated bedrock and erratic blocks using cosmogenic ^{3}He and ^{21}Ne (personal communication from K. Hammerschmidt, 1999), and correlation with ^{14}C-dated glacier advances in adjacent Bolivia (Clayton and Clapperton, 1997) suggest that the glaciers investigated here are Late-glacial in age. The fresh geomorphological forms show that postglacial erosion was minimal.

Two climate stations, operated by the Dirección General de Aguas, Chile, are located close to the case-study areas and provide several years of data (1984–94): station El Tatio (22° 21′ S, 68° 02′ W; 4320 m a.s.l.) and station Chungará Ayata (18° 14′ S, 69° 07′ W; 4570 m a.s.l.) (Fig. 1; Table 1). Additional data are taken from two automatic weather stations slightly further south at El Laco (23° 50′ S, 67° 29′ W; data 1990–94) at 4500 and 5000 m a.s.l., where Vuille (1996) established statistical–empirical models for melt and sublimation rates as a

https://doi.org/10.3189/172756500781832611 Published online by Cambridge University Press

function of climate. These models were developed by multiple regression analysis on different test sites, and allow daily determination of sublimation and melt rates with a high degree of confidence (r^2 for the sublimation model = 0.9; r^2 for the melt model = 0.8). Although this statistical–empirical approach cannot describe the melt process physically, it proved useful for our purposes, and calculates the daily melting rates well, since global radiation in this area is the controlling factor for the daily temperature cycle and thus for melt. Field measurements and climate data from Glaciar Zongo, Bolivia (16° S, 68° W; Sicart and others, 1998; Wagnon and others, 1999), provide the frame for the melt and sublimation terms of a glacier under (sub)tropical conditions.

4. METHODOLOGY

4.1. Mass-balance and climate modeling

The actualistic principle (assumption that the modern processes were the same and active also in the past) is used as a basis and prerequisite for mass-balance modeling as a function of climate. The respective empirical–statistical models for this area were established by Vuille (1996) and Kull (1999), and are listed in Table 2A and B.

The modeling scheme is shown in Figure 2 (for a detailed discussion see Kull, 1999). Annual and daily amplitudes, mean values and lapse rates were calculated from station data for the parameters temperature (T), relative humidity (RH), wind velocity (W), global radiation (G), cloudiness (C) and precipitation (P). Correction terms for ΔT as a function of C and P, and ΔG (as a function of C and "topography" (shielding)) were determined individually with climate data, and allowed us to parameterize the local climate on an hourly basis for the summer (October–March), and on a daily basis for the winter (Table 2A; Kull, 1999). In the Late-glacial climate scenario, G is corrected for the changing Earth orbital parameters (Blatter and others, 1984). Ammann (1996) established a correlation model for this area which describes the correlation between "cloudiness" and "precipitation". As shown in Figure 3, the model climate averaged for the winter and summer compares well with the station data. Melt, sublimation and accumulation rates are quantified as a function of the respective climate conditions and the degree-day factor (DDF) which is variable and depends on snow characteristics, climate and season (Vuille, 1996; Kull, 1999; Fig. 2; Tables 1 and 2A). DDF is calibrated for the dry cold winter conditions in the research area (Vuille, 1996) and for humid warm summer conditions on Glaciar Zongo (Sicart and others, 1998; Kull, 1999; Wagnon and others, 1999). In order to account for the influence of the former glacier on the local climate, the air temperatures in our test areas were corrected using climatic data from Glaciar Zongo, where Sicart and others (1998) and Wagnon and others (1999) compared air temperatures on the glacier and on adjacent lateral moraines. Thus a value of $dT = -2$°C is applied to calculate local air temperatures on glaciated surfaces from station data in our currently ice-free test areas (Kull, 1999). Subsequently, the mass-balance terms are calculated for individual altitudinal segments of the glacier, and the mass flow is calculated after Oerlemans (1997; Table 2C) for given cross-sections within the reconstructed glacier bed. Finally, the paleoclimate scenario is tuned (iteration, Fig. 2) such that the model glacier is in steady state, in equilibrium with the paleoclimate, matches the observed glacier geometry and thus fulfills two conditions:

Table 1. Modern climatic conditions at weather stations in both case-study areas. The lapse rates are calculated per 100 m elevation

	El Tatio	*Choquelimpie*
Temperature (°C)		
Annual mean	3.6[b]	4.2[a]
Annual amplitude	3.7[b]	2.7[a]
Lapse rate	−0.68 ± 0.03[e]	−0.68 ± 0.03[e]
Precipitation (mm)		
Annual mean	250[e]	340[a]
Winter	70[e]	35[a]
Lapse rate	12[e]	12[e]
Global radiation (W m^{-2})		
Annual mean	273.75[d]	250.83[a]
Annual amplitude	62.5[d]	43.33[a]
Lapse rate	1.67[e]	1.67[e]
Cloudiness (%)		
Annual mean	20[g]	25[g]
Annual amplitude	10[g]	15[g]
Lapse rate	0.84[g]	0.84[g]
Wind (m s^{-1})		
Annual mean	7.05[d]	7.05[d]
Annual amplitude	2[d]	2[d]
Lapse rate	0.08[c,d]	0.08[c,d]
Rel. humidity (%)		
Annual mean	34[b]	58[a]
Annual amplitude	15[b]	10[a]
Lapse rate	0.09[c,d]	0.09[c,d]
Deg.-day factor (mm °C^{-1} d^{-1})		
Annual mean	4.5[e,f]	4.5[e,f]
Annual amplitude	2.5[e,f]	2.5[e,f]
Lapse rate	−0.09[e,f]	−0.09[e,f]

[a] Chungará Ayata station (18° 14′ S, 69° 20′ W; 4570 m a.s.l.; 1984–94).
[b] El Tatio station (22° 21′ S, 68° 02′ W; 4320 m a.s.l.; 1977–94).
[c] El Laco station (23° 50′ S, 67° 29′ W; 4400 m a.s.l.; 1990–94).
[d] El Laco station (23° 50′ S, 67° 29′ W; 5000 m a.s.l.; 1990–94).
[e] Vuille (1996).
[f] Sicart and others (1998), Wagnon and others (1999).
[g] Ammann (1996).

(1) total overall mass balance of the glacier (annual average) = 0.

$$0 = \sum_{\Delta h} (b_h A_h)\,, \qquad (1)$$

where Δh are the elevation zones (m a.s.l.) of the reconstructed glacier surface, b_h is the specific annual balance (kg m^{-2}) of a given altitudinal zone and A_h is the glacier surface (m^2) of a given altitudinal zone.

(2) difference between mass influx into a cross-section and the total mass balance below the cross-section (DMM) = 0 for individual cross-sections in the glacier valley.

$$\mathrm{DMM}_{\mathrm{cr1}/2} = \sum_{\Delta h=0}^{h_{\mathrm{cr1}/2}} (b_h A_h) + \mathrm{M}_{\mathrm{cr1}/2} = 0\,, \qquad (2)$$

where $\mathrm{DMM}_{\mathrm{cr1}/2}$ is the difference (kg a^{-1}) between annual mass influx in a cross-section and mass balance below the cross-section, $h_{\mathrm{cr1}/2}$ is the altitudinal zone (m a.s.l.) of a cross-section, and $\mathrm{M}_{\mathrm{cr1}/2}$ is the mass influx (kg a^{-1}) in a cross-section (Table 2C).

https://doi.org/10.3189/172756500781832611 Published online by Cambridge University Press

Table 2. (A) Parameterization for the daily, annual cycles, amplitudes of the climate and correction factors for temperature and global radiation. (B) Empirical–statistical models developed in the research area for the mass-balance modeling. (C) Equations for the ice-flow and mass-flux calculation for the considered cross-sections in the two case-study glaciers

A. *Climate*:

Temperature[a,d,f]	$T_{t,h}$ (°C):	$T_{t,h} = \mathrm{Ym} + \mathrm{Ya}\,(\cos d) + \mathrm{Da} + C^{*})\cos t + \mathrm{grad}_h + P^{*}$	
Cloudiness[c]	$\mathrm{Cs}_{t,h}$ (%): (summer)	$\mathrm{Cs}_{t,h} = \mathrm{Ym} + \mathrm{Ya}\,(\cos d_\mathrm{s}) + \mathrm{Da}(\cos t_\mathrm{s}) + \mathrm{grad}_h$;	$0 < \mathrm{Cs} < 100$
	$\mathrm{Cw}_{t,h}$ (%): (winter)	$\mathrm{Cw}_{t,h} = \mathrm{Wm} + \mathrm{Wa}\,(\sin d_\mathrm{w}) + \mathrm{grad}_h$;	$0 < \mathrm{Cw} < 100$
Precipitation[c,d,f]	$\mathrm{Ps}_{t,h}$ (mm): (summer)	$\mathrm{Ps}_{t,h} = 0.161\mathrm{Cs}_{t,h}{}^2 + 0.81\mathrm{Cs}_{t,h} + \mathrm{grad}_h$	
	$\mathrm{Pw}_{t,h}$ (mm): (winter)	$\mathrm{Pw}_{t,h} = \mathrm{Wm}(\mathrm{Cw}_{t,h}\mathrm{Wm}^{-1}) + \mathrm{grad}_h$	
Rel. humidity[a,b,f]	$\mathrm{RH}_{t,h}$ (%):	$\mathrm{RH}_{t,h} = \mathrm{Cs}_{t,h} + \mathrm{Cw}_{t,h} + \mathrm{grad}_h$	
Wind speed[b]	$\mathrm{W}_{d,h}$ ($\mathrm{m\,s^{-1}}$):	$\mathrm{W}_{d,h} = \mathrm{Ym} + \mathrm{Ya}\,(\sin d) + \mathrm{grad}_h$	
Global radiation[b,d]	$\mathrm{G}_{d,h}$ ($\mathrm{W\,m^{-2}}$):	$\mathrm{G}_{d,h} = \mathrm{Ym} + \mathrm{Ya}\,(\cos d) + C^{*} + T^{*} + \mathrm{grad}_h$	
Deg.-day factor[d,e]	$\mathrm{DDF}_{d,h}$ ($\mathrm{mm\,°C^{-1}\,d^{-1}}$):	$\mathrm{DDF}_{d,h} = \mathrm{Ym} + \mathrm{Ya}\,(\cos d)\cos h + \mathrm{grad}_h \sin h$	

Corrections:

Temperature	P^{*}[a]: Correction term due to precipitation, $\Delta T = 4$°C if $P > 0$
	C^{*}[a]: Correction term due to cloudiness, $\Delta\mathrm{Da} = -0.03\,C$ (%).
Global radiation energy	P^{*}[b]: Correction term due to cloudiness, $\Delta G = -0.25\,C$ (%)
	T^{*}: Correction term due to radiation shielding (topography).

Da:	daily amplitude	Ya:	annual amplitude	Ym:	annual mean value	grad_h:	lapse rate (h (100 m)$^{-1}$)
P^{*}:	precipitation corr.	T^{*}:	topographic corr.	Wm:	winter mean value	Wa:	winter amplitude
t:	hours	h:	altitude	d:	days ($f(t)$)	t_s:	hours in summer

C^{*}	cloudiness corr.
d_s	days in summer (Oct–Mar) ($f(t)$)
d_w	days in winter (Apr–Sep) ($f(t)$)

[a] El Tatio (4320 m a.s.l.; 22°21′ S, 68°02′ W; 1977–94).
[b] El Laco (5000 m a.s.l.; 23°50′ S, 67°29′ W; 1990–94).
[c] Ammann (1996).
[d] Vuille (1996).
[e] Sicart and others (1998), Wagnon and others (1999).
[f] Chungará Ayata (4570 m a.s.l.; 18°14′ S, 69°20′ W; 1984–94).

B. *Mass balance*:

Sublimation[a]

$$\mathrm{subl}_{l,h} = -1.33 + 0.12(W_{d,h}) + 0.24(Dd_{d,h}) + 0.27(G_{d,h}) \quad (\mathrm{mm\,d^{-1}})$$

with:	$W_{d,h}$:	max. hourly wind velocity (daily average)	($\mathrm{m\,s^{-1}}$)
	$Dd_{d,h}$:	mean daily vapour-pressure deficit	(hPa $\mathrm{d^{-1}}$)
	$G_{d,h}$:	daily global radiation energy	($\mathrm{W\,m^{-2}}$)

Melt[a]

$$\mathrm{melt}_{d,h} = 0.97 + \mathrm{DDF_{d,h}}(\mathrm{Tg_{t,h}})\,; \quad \text{for} \quad \mathrm{Tg} > 0 \qquad (\mathrm{mm\,d^{-1}})$$

with:	$\mathrm{Tg}_{t,h}$:	hourly means of the positive temperatures per day	(°C)
	$\mathrm{DDF}_{d,h}$:	degree-day factor, f (albedo, snow density, climate)	($\mathrm{mm\,°C^{-1}\,d^{-1}}$)

Accumulation[b] ($\mathrm{mm\,d^{-1}}$)

$$\mathrm{acc}_{d,h} = \frac{1}{24}\sum_{t=24d}^{24+24d}\begin{bmatrix} P_{t,h} & \text{if} \quad T_{t,h} < 2 \\ \left(\dfrac{4 - T_{t,h}}{2}\right)P_{t,h}\,; & \text{if} \quad 2 \le T_{t,h} \le 4 \\ 0 \text{ otherwise} & \end{bmatrix}$$

with:	$P_{t,h}$:	hourly precipitation	(mm)
	$T_{t,h}$:	hourly mean temperature	(°C)

Specific annual mass balance $b_\mathrm{h} = \sum_d -(\mathrm{subl}_{d,h} + \mathrm{melt}_{d,h}) + \mathrm{acc}_{d,h}$ ($\mathrm{mm\,a^{-1}}$)

[a] Vuille (1996).
[b] Kull (1999).

C. *Ice flow*:

Flow velocity[a]

$$U = U_\mathrm{d} + U_\mathrm{s} = f_\mathrm{d} H\tau^3 + \frac{f_\mathrm{s}\tau^3}{H} \quad (\mathrm{m\,s^{-1}})$$

with:	$\tau = -F\rho g H\beta$ = mean basal shear stress in cross-section[b]	(Pa)
	$F = (Q/HB)$ = form factor[c]	(%)
	Q = cross-section area	($\mathrm{m^2}$)
	B = hydraulic radius	(m)
	U = mean ice velocity in the cross-section	($\mathrm{m\,s^{-1}}$)
	U_d = deformation velocity	($\mathrm{m\,s^{-1}}$)
	U_s = sliding velocity	($\mathrm{m\,s^{-1}}$)
	f_d = flow parameter (internal deformation)	($1.9 \times 10^{-24}\,\mathrm{Pa^{-3}\,s^{-1}}$)
	f_s = flow parameter (basal sliding)	($5.7 \times 10^{-20}\,\mathrm{Pa^{-3}\,m^2\,s^{-1}}$)
	H = ice thickness	(m)
	ρ = ice density	($900\,\mathrm{kg\,m^{-3}}$)
	g = acceleration due to gravity	($\mathrm{m\,s^{-2}}$)
	β = bed slope	(%)

Cross-section mass influx $M = UQ\rho$ ($\mathrm{kg\,s^{-1}}$)

[a] Oerlemans (1997).
[b] Paterson (1994).
[c] Budd (1969).

https://doi.org/10.3189/172756500781832611 Published online by Cambridge University Press

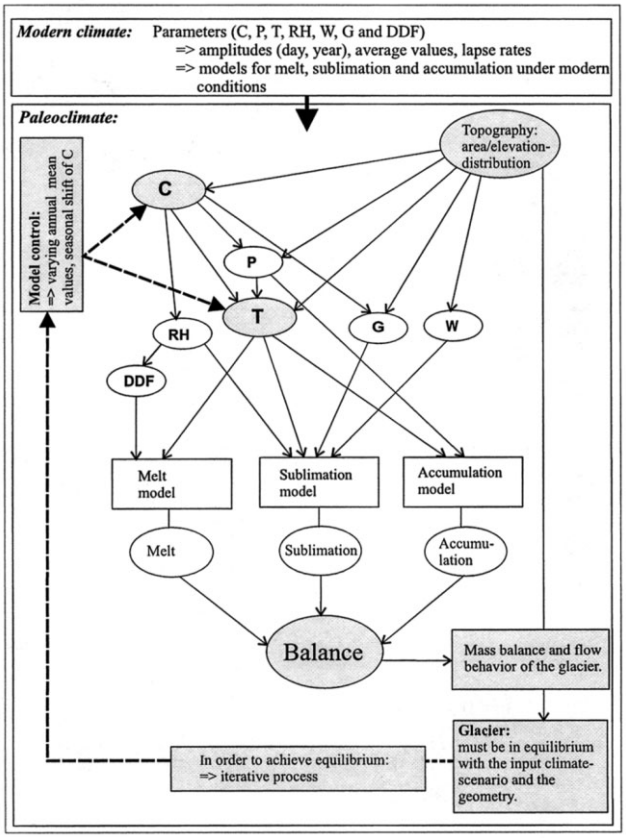

Fig. 2. Flow chart of the climate–glacier model (Kull, 1999) with cloudiness C, temperature T, precipitation P, relative humidity RH*, global radiation energy G and wind velocity W. The degree-day factor (DDF) is variable and depends on the respective seasonal climate conditions. C regulates* RH*, P, T and G to a considerable degree, whereas the accumulation and ablation modules are largely controlled by T, P,G, W and* RH*. Thus the principal climate parameters which govern the climate scenario and control the model are C and T.*

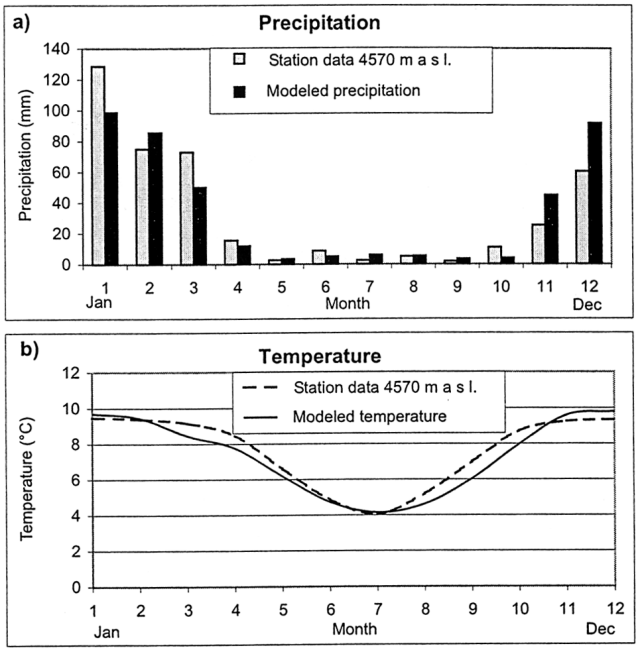

Fig. 3. Comparison of precipitation and temperature values (monthly mean) between station Chungará Ayata (18° 14′ S, 69° 07′ W; 4570 m a.s.l.; Table 1) and the model climate for the same location. The model climate data were calculated using the station data (Table 1) and the parameterization shown in Table 2A.

Fulfillment of both equations results in steady-state conditions of a glacier. Figure 4a and d show the temperature–precipitation diagrams for both case-study areas with numerical solution for Equation (1) (overall mass balance = 0), which is a prerequisite for the subsequent calculations. Figure 4b, c, e and f show the respective differences between the mass influx and the mass balance below each of the two considered cross-sections (DMM values Equation (2), fulfillment of Equation (1) as calculated using the climate scenarios where the temperature–precipitation combinations fulfill condition 1 (Fig. 4a and d)). For steady-state conditions of the glacier, DMM values must be zero (Equation (2)). In general, DMM decreases with increasing precipitation and temperature, because higher precipitation requires higher temperatures in order to fulfill Equation (1). Also mass-balance gradients increase, resulting in more negative mass-balance values below the considered cross-sections.

Because the bed geometry at the considered cross-sections is field-measured, the only parameters not defined for calculating the mass influx into a cross-section are the ice-flow parameters. Using standard ice-flow parameters (Table 2c), it appears from Figure 4 that $\mathrm{DMM}_{\mathrm{cr1/2}} = 0$. Figure 4b, c, e and f also show that there is only one numerical solution ($\mathrm{DMM}_{\mathrm{cr1}} = \mathrm{DMM}_{\mathrm{cr2}} = 0$) with one particular combination of "temperature" and "precipitation" (and all the other dependent climatic variables (Fig. 2)) which fulfills Equations (1) and (2), matches the observed paleoglacier geometry and is thus the most likely paleoclimate reconstruction (for discussion see section 5).

4.2. Sensitivity of the model

It appears from Figure 4b, c, e and f that the uncertainty of the paleoclimate scenario is ultimately determined by the DMM values of the cross-sections (Equation (2)), which in turn are controlled by two groups of data: (i) geometrical data based on field measurements and (ii) ice-flow parameters from experimental data (standard values, Table 3a).

We allowed an error of ±5% for the mapped geometrical data (ice height H and bed width B at two cross-sections, valley slope β) and for the standard ice-flow parameters ($f_{\mathrm{d}}, f_{\mathrm{s}}$). As shown in Table 3b, ±5% changes in geometrical or flow parameters result in $\Delta\mathrm{DMM}_{\mathrm{cr1/cr2}}$ ($\mathrm{DMM}_{\mathrm{cr1/cr2}} \neq 0$) variations between $+0.5/-0.6 \times 10^6\,\mathrm{kg\,a^{-1}}$. Thus we allow this range of $\Delta\mathrm{DMM}_{\mathrm{cr1/cr2}}$ as a possible numerical solution for a paleoclimate scenario (Table 4; shaded range in Fig. 7a and b).

Whereas the geometry of the glacier bed at the cross-sections is well defined, the ice-flow parameters remain debatable to some extent. However, using extreme changes in the order of ±50% from standard ice-flow parameters results in an increase of $\Delta\mathrm{DMM}_{\mathrm{cr1/cr2}}$ values to $+18 \times 10^6\,\mathrm{kg\,a^{-1}}$ and $-10 \times 10^6\,\mathrm{kg\,a^{-1}}$ for both test areas, and no numerical solution for Equations (1) and (2) is found within the observed glacier geometry. Only ice-flow parameters within the range of ±5% from standard values yield numerical results for Equations (1) and (2) which are compatible with the observed geometry (range ±5%).

In order to validate our empirical–statistical approach, we compared our model (mass-balance modeling) with a physical energy-balance model. H. Oerlemans (personal communication, 1998) used our modeled best-fit paleoclimate scenario for El Tatio as input climate scenario for his physical mass-balance model and showed that the resulting mean

https://doi.org/10.3189/172756500781832611 Published online by Cambridge University Press

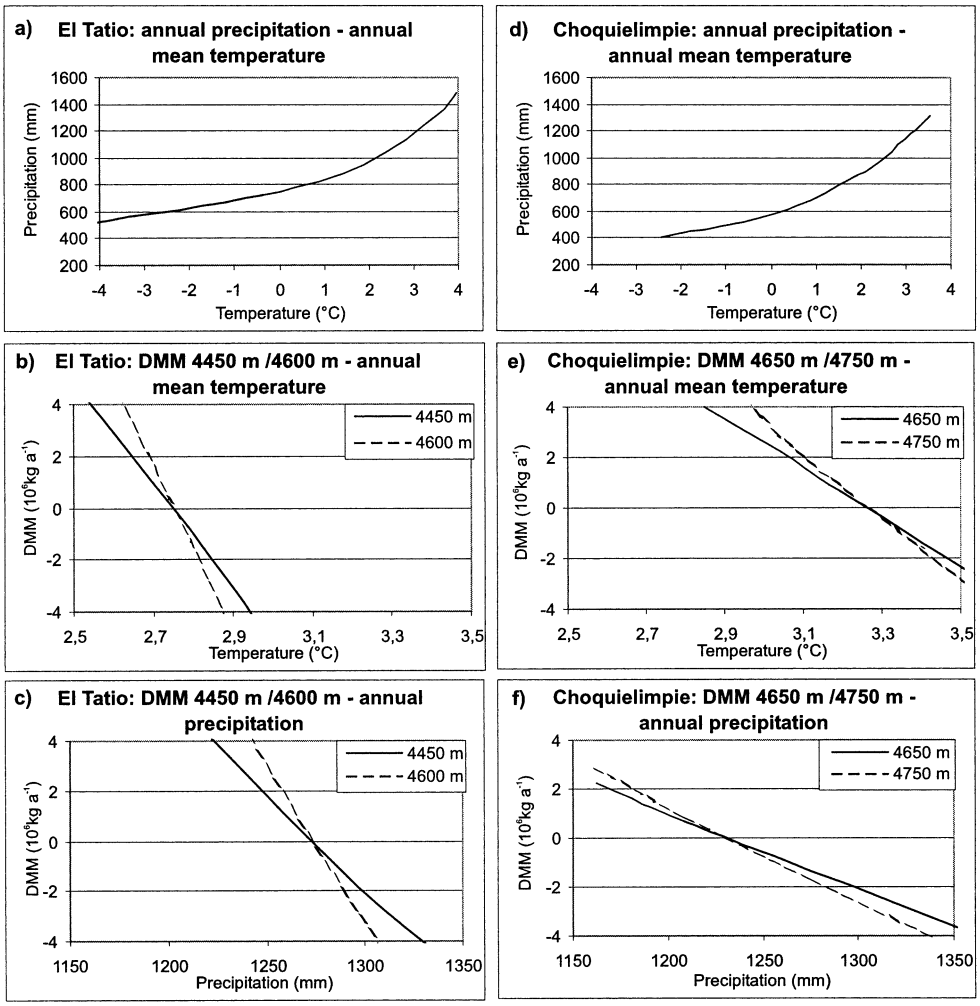

*Fig. 4. (a, d) Temperature–precipitation diagrams for both case-study glaciers, showing the numerical solutions for total mass balance = 0 (Equation (1)). P and T refer to 4000 m altitude. (b, c, e, f) Differences between the mass influx and the total mass balance below the respective cross-sections (*DMM*) as a function of temperature (b, e) or as a function of precipitation (c, f).* DMM = *0 in both cross-sections fulfills Equation (2) for steady-state conditions of a glacier and provides the numerical solution for the P climate scenario which matches the observed glacier geometry.*

annual mass balance of the whole glacier is close to zero (fulfilling Equation (1)) and thus in agreement with our results.

5. RESULTS AND DISCUSSION

5.1. Modern glaciological conditions

In a first step, we tested the suitability of our climate–glacier model for modern climatic and glaciological conditions in the case-study areas. The results (Fig. 5) compare favorably with the field data and show the major characteristic glaciological features of today. In the southern case-study area of El Tatio at 22° S (Fig. 5a), the calculated mass balance is negative in all the altitudinal zones up to 6000 m. This is in agreement with field observations, confirming that the modern climate is too arid to sustain glaciers even in the continuous permafrost belt above 5600 m. Peaks as high as 6176 m (Volcán Aucanquilcha (21°13′ S) and Cerro Pili (23°17′ S; 6040 m a.s.l.) are currently free of glaciers and perennial snowfields, so no ELA currently exists. In the slightly more humid and warmer northern test area at Choquelimpie (18° S, Fig. 5b), the annual mass balance changes to positive values above altitudes of 5850 m, suggesting that there is enough moisture to sustain glaciers at high altitudes. However, the humidity is still at critically low levels. Indeed, the highest peaks in this area such as Volcán Sajama (6542 m) and Parinacota (6200 m) show ice caps with modern ELAs at about 5800 m (Hastenrath, 1971; Jordan, 1991), and glacier tongues as low as about 5200 m on the southwest-facing slope (comparable to the case-study glacier at Choquelimpie). Interestingly, peaks at about 6000 m (such as Guaillatiri (6024 m)) still exhibit small snow/firn patches, whereas nearby Volcán Tacora (5980 m) and all the other peaks below 5800 m are currently free of glaciers.

We conclude from the good comparison between calculated and observed modern ELAs that the statistical–empirical models which link climate data with sublimation, melt and accumulation terms (Vuille, 1996; Kull, 1999) are suitable for both case-study areas.

5.2. Late-glacial climate conditions

Here, we use the climate–glacier model to reconstruct paleoclimatic conditions from two late Pleistocene case-study glaciers with well-known geometries of the former ice mass, assuming steady-state conditions of the glacier. Table 4 lists the results of the paleoclimate reconstruction (best numerical solution) reduced to 4000 m a.s.l., and Figure 6 shows the respective mass-balance terms in different altitudinal belts. In this first step the paleoclimate scenario is based on the assumption that the seasonality of precipitation is compar-

https://doi.org/10.3189/172756500781832611 Published online by Cambridge University Press

Table 3. (A) Geometry of both case-study glaciers with the altitudes of cross-sections 1 and 2 $\mathrm{cr}_{1,2}$*, the lengths of the tongue below the cross-section* X*, ice height at the cross-section* H*, cross-section area* A*, mean valley slope* β*, ice-flow parameters for basal sliding* f_s*, and internal deformation* f_d*. Using the best-fit paleoclimate scenario (Table 4), the combination of the parameters yields the exact numerical solution for* $\mathrm{DMM}_{\mathrm{cr}_{1,2}} = 0$*. (B) Sensitivity of* $\Delta\mathrm{DMM}_{\mathrm{cr}_{1,2}}$ *(*$\mathrm{DMM}_{\mathrm{cr}_{1,2}} \neq 0$*) to ±5% change in the geometrical parameters (ice height at cross-section* H*, bed width at cross-section* B*, mean valley slope* β*) and ice-flow parameters (basal sliding* f_s *and internal deformation* f_d*)*

A.

cr_1	cr_2	X_1	X_2	H_1	H_2	A_{cr_1}	A_{cr_2}	β	f_s[a]	f_d[a]	DMM
m a.s.l.	m a.s.l.	m	m	m	m	m^2	m^2	%	$Pa^{-3}\,m^2\,s^{-1}$	$Pa^{-3}\,s^{-1}$	$10^6\,kg\,a^{-1}$
El Tatio:											
4450	4600	2600	4500	115	120	45 425	90 080	0.094	5.7×10^{-20}	1.9×10^{-24}	0
Choquielimpie:											
4650	4750	2250	4000	110	115	96 750	109 375	0.046	5.7×10^{-20}	1.9×10^{-24}	0

B.

	$H_1, H_2 \pm 5\%$	$B_{\mathrm{cr}_1,\mathrm{cr}_2} \pm 5\%$	$\beta \pm 5\%$	$f_s \pm 5\%$	$f_d \pm 5\%$
Sensitivity El Tatio:					
$\Delta\mathrm{DMM}_{\mathrm{cr}_1/\mathrm{cr}_2}$	+0.44	+0.32	+0.46	+0.32	+0.37
$10^6\,kg\,a^{-1}$	−0.37	−0.49	−0.59	−0.53	−0.60
Sensitivity Choquielimpie:					
$\Delta\mathrm{DMM}_{\mathrm{cr}_1/\mathrm{cr}_2}$	+0.50	+0.42	+0.49	+0.48	+0.50
$10^6\,kg\,a^{-1}$	−0.21	−0.58	−0.60	−0.2153	−0.28

[a] Oerlemans (1997).

Table 4. Best-fit late Pleistocene climate scenario and glaciological conditions for both case-study glaciers calculated for 4000 m a.s.l.

	Choquielimpie	Δ *change values*	*El Tatio*	Δ *change values*
Temperature (°C)				
Annual mean	3.2 (−0.1/+0.2)	*−4.4 (−0.1/+0.2)*	2.6 (−0.1/+0.1)	*−3.2 (−0.1/+0.1)*
Precipitation (mm)				
Annual mean	1250 (−50/+10)	*+840 (−50/+10)*	1280 (−10/+30)	*+1000 (−10/+30)*
Winter 4 month	25 (−25/+155)	*−10 (−25/+155)*	100 (−75/+100)	*+30 (−75/+100)*
Winter %	5 (−5/+10)	*−3 (−5/+10)*	8 (−6/+7)	*−12 (−6/+7)*
Winter 6 month	200 (−200/+200)	*+165 (−200/+200)*	400 (−100/+200)	*+330 (−100/+200)*
Winter %	15 (−15/+17)		30 (−8/+20)	
Rel. humidity (%)				
Annual mean	52 (−3/+8)	*+4 (−3/+8)*	52 (−3/+8)	*+18 (−3/+8)*
Winter 6 month	20 (−2/+15)	*−25 (−2/+15)*	24 (−2/+15)	*0 (−2/+12)*
Summer	85 (−25/+2)	*+47 (−25/+2)*	80 (−30/+2)	*+31 (−30/+2)*
Global radiation ($W\,m^{-2}$)				
Annual mean	158 (−16.6/+4.2)	*−91.6 (−16.6/+4.2)*	158 (−16.6/+4.2)	*−112.5 (−16.6/+4.2)*
Winter 6 month	208 (−25/+12.5)	*−4.2 (−25/+12.5)*	204 (−20.8/+12.5)	*−4.2 (−20.8/+12.5)*
Summer	108 (−4.2/+33.3)	*−141 (−4.2/+33.3)*	112 (−4.2/+37.5)	*−158.3 (−4.2/+37.5)*
Cloudiness (%)				
Annual mean	48 (−3/+12)	*+23 (−3/+12)*	50 (−2/+15)	*+30 (−2/+15)*
Winter 6 month	12 (−7/+18)	*−3 (−7/+18)*	15 (−5/+15)	*+5 (−5/+15)*
Summer	85 (−25/+5)	*+45 (−25/+5)*	84 (−30/+5)	*+54 (−30/+5)*
ELA				
m a.s.l.	4903 (−3/+7)	*−950*	4830 (−2/+8)	
ρ_{ELA} (mm)	1360 (−40/+20)		1390 (−40/+10)	
t_{ELA} (°C)	−2.6 (−0.1/+0.2)		−2.7 (−0.1/+0.2)	
AAR	0.61 (−0.01/+0.02)		0.66 (−0.015/+0.01)	
Mass-bal.grad. (abl. area ($kg\,m^{-2}\,m^{-1}$)	8.9 (−0.05/+0.3)		8.8 (−0.5/+0.2)	

Note: The given range is based on the sensitivity of $\mathrm{DMM}_{\mathrm{cr}_{1,2}}$ to the respective changes in the geometry (±5%) and in the ice-flow parameters (±5%, Table 3).

https://doi.org/10.3189/172756500781832611 Published online by Cambridge University Press

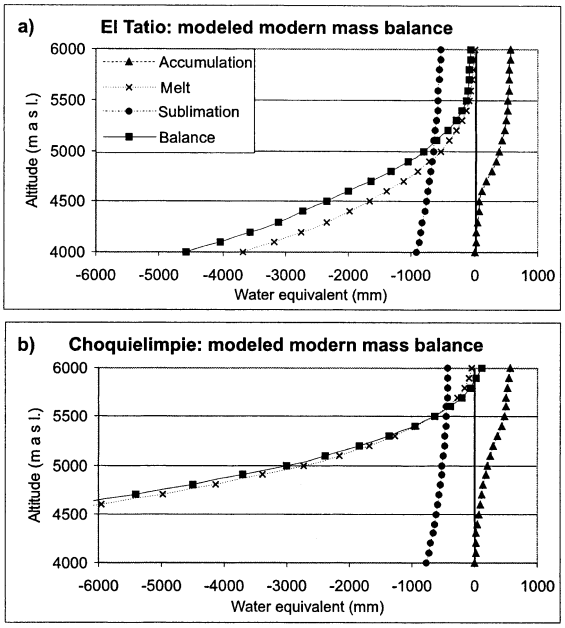

Fig. 5. Model results for mass-balance terms at different altitudes for both hypothetical case-study glaciers under modern climate conditions (station data, Table 1). In the southern test area at 22° S, El Tatio, the mass balance is negative up to 6000 m a.s.l., confirming the lack of glaciers even in the continuous permafrost belt. In the northern test area at 18° S, Choquielimpie, the mass balance turns to positive values above 5850 m altitude, effectively reflecting the existence of small glaciers on peaks higher than 6000 m. Cerro Choquielimpie (5327 m) is currently ice-free.

able to the modern situation (i.e. predominantly tropical summer precipitation).

The results from the case-study areas at El Tatio and Choquielimpie are in good agreement. Accounting for a ±5% margin of uncertainty in the geometry of the glacier, the model suggests a depression of the mean annual temperature of 4.4 (−0.1/+0.2) °C, and an increase in annual precipitation rates in the order of 840 (−50/+10) mm for the northern test area at 18° S. The results for the southern test area at 22° S show a mean annual temperature depression in the order of 3.2 (±0.1) °C and an annual precipitation increase of 1000 (−10/+30) mm (see Table 4). The vertical distribution of the annual mass-balance terms (Fig. 6a and d) suggests a Pleistocene ELA at 4900 m (Choquielimpie) and at 4830 m (El Tatio), which is about 50 m higher than the Pleistocene ELA inferred from field data (starting-point of lateral moraines; Jenny and Kammer, 1996). In the northern area, the Pleistocene depression of the ELA amounts to approximately 1000 m, which is comparable with the range 800–1200 m reported for adjacent areas in Bolivia and Peru (Hastenrath, 1967, 1971; Graf, 1991; Klein and others, 1999). The model also suggests an accumulation-area ratio (AAR) of 0.61–0.66 for the Pleistocene glaciers, which agrees with field data (Jenny and Kammer, 1996).

Figure 6b, c, e and f show the mass-balance terms separated for the summer and winter seasons. Typically for (sub)-tropical glaciers, the main ablation period coincides with the main accumulation period during summer. On the other hand, this effectively reflects the cold, dry climate conditions during winter, when the major proportion of the energy available for ablation is consumed for sublimation. Sublimation is approximately eight times more energy-intensive than melting and is the dominant ablation term at high altitudes during winter in this climate. Thus Pleistocene summer mass-balance gradients in the ablation area (about 12 kg m^{-2} m^{-1}) are greater than winter values (about 4 kg m^{-2} m^{-1}) and compare favorably with values for (sub)tropical glaciers (Kaser and others, 1996; Kaser and Georges, 1999). The annual mean value is 8.8–9.2 kg m^{-2} m^{-1}. Interestingly, both seasonal extremes (~12 kg m^{-2} m^{-1} during summer, ~4 kg m^{-2} m^{-1} during winter) result in a mean annual mass-balance gradient and, finally, in an AAR which is close to values for alpine glaciers in oceanic climates of mid-latitudes (AAR 0.66, mass-balance gradient 7.7 kg m^{-2} m^{-1}; Kaser, 1996). These modeling results are in agreement with the field data (AAR of 0.66) by Jenny and Kammer (1996).

The inferred Late-glacial temperature depressions of 4.4 (−0.1/+0.2) °C for the northern test area at 18° S, and 3.2 (±0.1) °C for the southern test area at 22° S compare favorably with results from glaciological studies in adjacent areas of Bolivia and Peru (Seltzer, 1992, 1993; Clayton and Clapperton, 1997). However, our results as well as the findings of Clayton and Clapperton (1997) suggest substantially higher precipitation (ΔP between +600 and +1000 mm) than the paleoclimate reconstruction from water-balance models of paleolakes (Hastenrath and Kutzbach, 1985; Kessler, 1985; Grosjean, 1994; ΔP around 300 mm). Given broad synchronicity between the paleolakes and the maximum glacier advances (Clayton and Clapperton, 1997), we might speculate about redeposition of snow in wind-protected glaciated valleys which would add to the accumulation of direct precipitation and affect the mass balance. Such processes are not likely for paleolakes. Preliminary data for net mass accumulation measured from a new ice core of Cerro Tapado at 30° S in Chile, and modern climate conditions (personal communication from P. Ginot, 1999) suggest additions of redeposited snow in the order of 100–200 mm a^{-1} w.e. on Glaciar Cerro Tapado, which is located in the wind-protected area of the mountain. Although nothing is known about this effect in the past, we consider such processes in the order of 100–200 mm a^{-1} as a possible explanation for the high values of total precipitation drawn from glacier–climate models in Late-glacial northern Chile.

We also emphasize that glaciers responded likely on a time-scale of decades to centuries to climate changes. Thus our climate reconstruction may reflect a relatively short period of maximum humid conditions with maximum ice expansions (the absolute age determination is still missing), whereas the ground-water-fed lakes responded at much larger time-scales and may not have recorded this event. Therefore, differences are expected between the climate reconstructions from glaciers and lakes.

We might also argue that mountains trigger local precipitation due to their topography. Glaciers would benefit directly from such local effects, whereas the water balance of paleolakes integrates regional precipitation patterns of the lake basin where such effects are subordinate. The mean altitude of a glacier is also substantially higher than the mean altitude of a paleolake basin, which, given a regional precipitation lapse rate of +12 mm per 100 m altitude, may explain a difference in the order of 100 mm a^{-1} between paleoclimate reconstructions from glaciers and paleolakes.

5.3. Late-glacial seasonality: winter or summer precipitation?

In section 5.1 and 5.2, the late Pleistocene climate reconstruc-

https://doi.org/10.3189/172756500781832611 Published online by Cambridge University Press

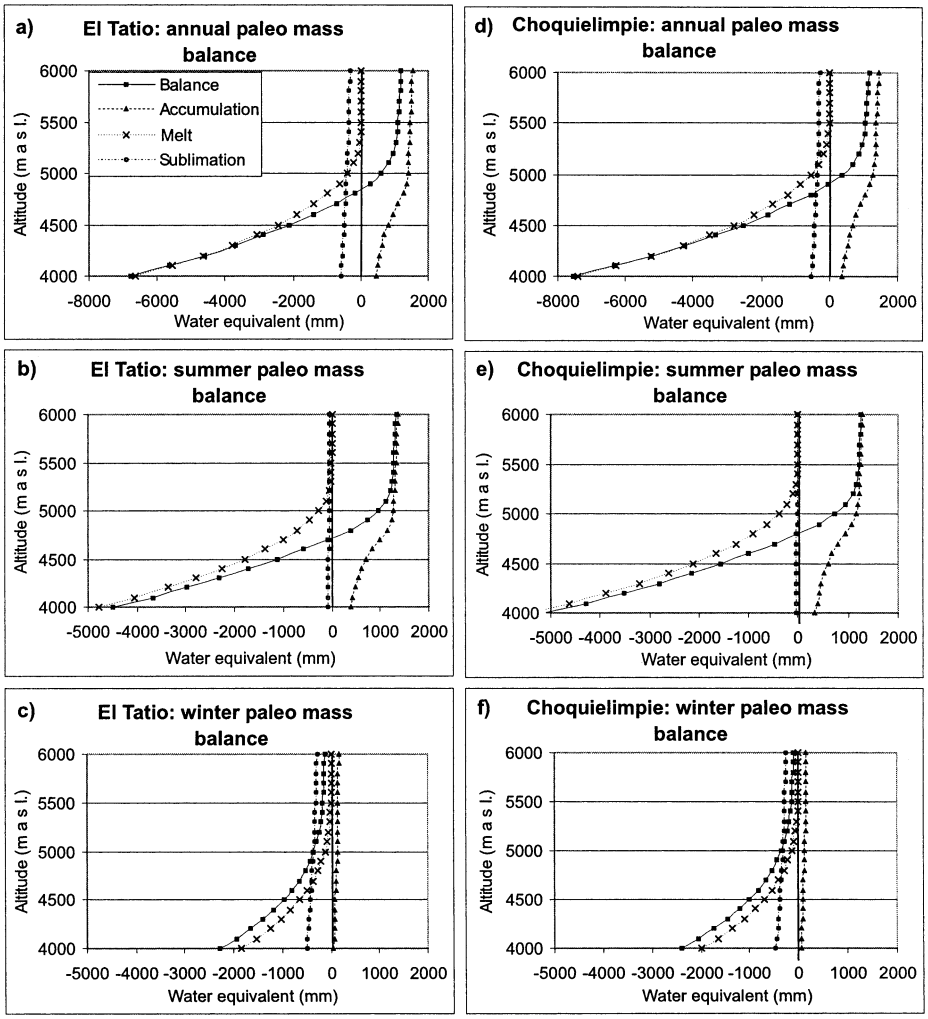

Fig. 6. Mass-balance terms for both case-study glaciers, calculated with the best-fit paleoclimate scenario for late Pleistocene (Late-glacial) times (Table 4). The ELA (specific annual mass balance = 0) is at 4830 m (El Tatio) and at 4900 m (Choquielimpie). Comparison between summer (b, e) and winter (c, f) shows significant differences. For (sub) tropical glaciers, summer is the main period for accumulation and ablation, whereas accumulation and ablation (mainly sublimation) are strongly reduced during the cold, dry winter season.

tions are based on the assumption that the seasonal distribution of precipitation remained similar to the modern situation, whereby approximately 80% of the precipitation falls during summer. This implies that the late Pleistocene increase in humidity is mainly explained by a reinforcement of the tropical precipitation belt. However, the source of the late Pleistocene humidity and hence the seasonality of precipitation remains a matter of debate (winter vs summer precipitation). Here, we use both case-study glaciers to test the hypothesis that reinforced extratropical winter precipitation may result in mass-balance terms and, ultimately, in a glacier geometry which matches the "real" geometry as observed in the field.

In our first scenario, winter precipitation increases during the 4 months June–September. Nowadays this is the typical season for episodic frontal precipitation penetrating into the case-study areas from the west wind belt (Pacific moisture source). Figure 7a (and Table 4) shows that the total amount of winter precipitation must not exceed 15% (180 mm a^{-1}) of the total annual precipitation, otherwise the geometry of the model glacier mismatches the field observation, again allowing for a measuring error of ±5%. Apparently, a winter precipitation scenario with high accumulation rates during winter and changed accumulation/ablation rates during the summer with mainly cloud-free conditions leads to different mass-balance gradients, and thus to a glacier with a geometry which differs from that observed in the field. Dry, cloud-free summer conditions favor energy-intensive sublimation compared to melt. This results in reduced mass-balance gradients and lower AARs. Such glaciers are currently found in the subtropical Andes at around 30° S in the extratropical winter precipitation regime. This finding has wide implications and suggests from the glaciological standpoint that a substantial increase in winter precipitation (June–September) must be discarded as a possible paleoclimate scenario for Late-glacial times.

However, there is, today at least, a second mechanism which brings Pacific moisture from the west wind circulation to the research area: isolated drops of cold polar air which migrate to lower latitudes and trigger precipitation when colliding with continental warm humid tropical air masses ("cut-off" events; Vuille and Ammann, 1997). These synoptic situations are typical for precipitation between the winter and the summer modes (i.e. in May–October) and involve the tropical and extratropical circulation belts. To account for these mechanisms, for the second scenario with increased winter precipitation we extended the period of precipitation to 6 months (May–October). Figure 7b (and Table 4) shows that the maximum proportion of winter precipitation increases markedly by 0–30% for Choquielimpie

https://doi.org/10.3189/172756500781832611 Published online by Cambridge University Press

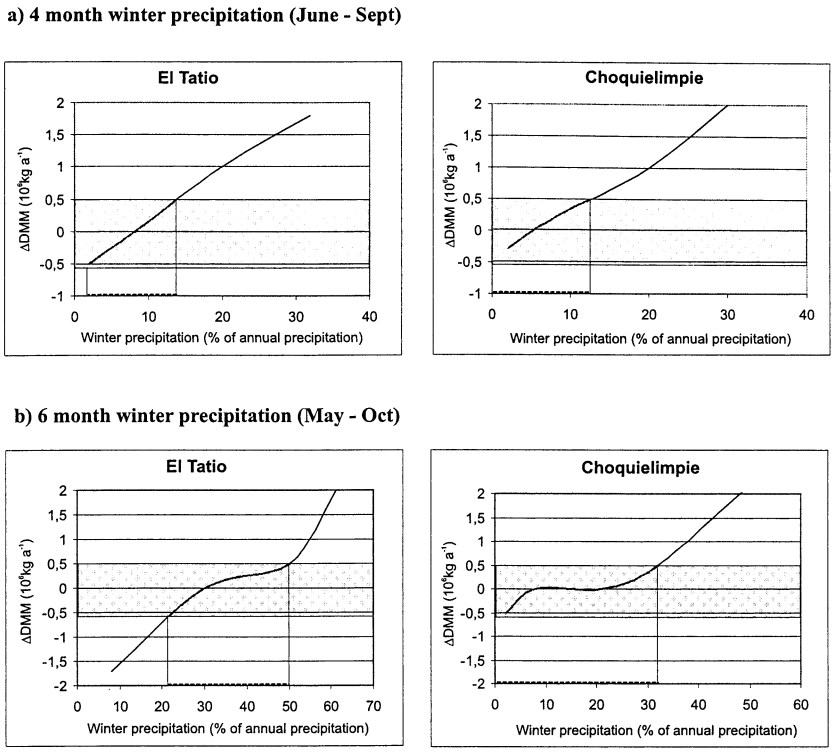

Fig. 7. $\Delta DMM_{cr1/cr2}$ ($DMM_{cr1/cr2} \neq 0$) *as a function of winter precipitation (% of total annual P). Based on the sensitivity test (±5% for geometrical parameters and flow parameters), we accept a range between* -0.6×10^6 *kg* a^{-1} *and* $+0.5 \times 10^6$ *kg* a^{-1} *(shaded area, dotted bar) as a possible numerical solution for a steady-state glacier. The scenario based on 4 months of winter precipitation (Fig. 7a) is indicative for frontal precipitation, whereas the scenario based on 6 months (Fig. 7b) includes frontal precipitation and "cut-off" events.*

and by 25–50% for El Tatio. This result points to the importance of precipitation during interseasonal periods (May and October) and to the potential significance of "cut-off" events during Late-glacial times. It is also found that these mechanisms were probably more important in the southern case-study area, El Tatio, than in the more tropical northern test area, Choquielimpie.

However, in terms of changes in the seasonal precipitation pattern, one might argue that the lapse rates and gradients of the climate parameters (used as input data for the model) are different for summer and winter precipitation regimes, and thus the actualistic principle (one of the prerequisites of our model) may not be appropriate. In particular, the lapse rates for precipitation are expected to vary substantially between convective summer precipitation and advective winter precipitation. Modern meteorological data show that there is no significant difference in the lapse rates of winter and summer precipitation on the isolated peaks in the research area. Hence this line of argument does not seem to question our conclusions.

In summary, our results suggest that the postulated increase in Late-glacial precipitation was mainly due to reinforced summer precipitation. This compares favorably with earlier findings from long-distance transported pollen, and spatial patterns of paleolake levels and ELA depressions (Kessler, 1991; Markgraf, 1993; Grosjean and others, 1995, 1996). A paleoclimate scenario based primarily on increased austral winter precipitation between June and September must be discarded as a possible explanation, but may, combined with precipitation of the "cut-off" type during the interseasonal months (May and October), account for up to 30% of the total annual precipitation in the northern test area, and 25–50% in the southern test area.

6. CONCLUSIONS

Widespread late Pleistocene glaciation provides evidence about significant climate changes in the currently ice- and glacier-free Andes of the Atacama Desert, northern Chile. We used a climate–glacier model to reconstruct paleoclimate conditions from two case-study glaciers at 18° and 22° S which reached their maximum advances during Late-glacial times. The model uses (i) detailed mapping of the Pleistocene glacier geometry, (ii) altitudinal gradients, diurnal and annual amplitudes and cycles of the modern climate, (iii) empirical–statistical sublimation, melt and accumulation models developed for this area, and (iv) dynamic ice flow through known cross-sections for steady-state conditions. In a first step we tested the model with modern climatic conditions. The results describe the modern glaciological conditions very well. In the fully arid southern case-study area at 22° S, El Tatio, the modeled mass balances are negative in all the altitudinal zones up to >6000 m, effectively reflecting the current conditions where there is a lack of glaciers and an ELA does not even exist in the continuous permafrost belt. In the warmer and more humid northern case-study area at 18° S, Choquielimpie, a modern ELA is calculated at 5850 m, which matches the field data and shows the critically low levels of available humidity which allow the southernmost glaciers of the tropical precipitation regime of the western Andes to survive. The good match with the modern situation validates our model for present-day-conditions.

For Late-glacial times, the model results suggest a substantial increase in precipitation ($\Delta P = +840$ (−50/+10) mm a^{-1} for the test area at 18° S; +1000 (−10/+30) mm a^{-1} for the test area at 22° S, compared to modern 250–450 mm a^{-1}), whereas the temperature depression remained relatively moderate

https://doi.org/10.3189/172756500781832611 Published online by Cambridge University Press

($\Delta T = -4.4\ (-0.1/+0.2)$ °C at 18° S; −3.2 (±0.1) °C at 22° S). This reinforces the view that Late-glacial glacier expansion and paleolake transgression was not primarily controlled by temperature (as in mid- and high-latitude areas), but rather by a substantial increase in effective moisture. This explains why the maximum glacier expansion in this area is not synchronous with the maximum glacier expansion in the mid- and high latitudes during the LGM at about 18 000 ^{14}C yr BP. Our results suggest that the increase in effective moisture is mainly due to reinforced tropical summer precipitation with Atlantic–continental moisture sources, i.e. comparable with modern climate conditions and seasonality. For a scenario based on frontal winter precipitation (restricted to the months June–September), the total amount of winter accumulation must not have exceeded 15% (180 mm a^{-1}) of the total annual precipitation, otherwise the geometry of the model glacier mismatches the field observation. If we allow 6 months of winter precipitation and include the typical precipitation mechanisms between the summer and the winter mode ("cut-off" events), the proportions of winter precipitation may reach 30% in the north (18° S) and 50% in the southern case-study area (22° S). Thus we suggest that the Late-glacial humidity changes in the central Andes were mainly controlled by changes in the tropical circulation pattern, whereas the extra-tropical westerly belt was not displaced equatorward. This seems to be very different from the Northern Hemisphere.

ACKNOWLEDGEMENTS

This study is part of the Swiss NSF project "Paleoclimate of the central Andes" (NF 20-056908.99) awarded to H. Veit. Methodical and logistical support by G. Kaser, H. Oerlemans, B. Pouyaud, P. Ribstein, H. Veit, B. Messerli and by M. Espinoza of Dirección Nacional de Fronteras y Límites del Estrado, Chile is gratefully acknowledged. We also thank S. Raper and R. van de Wal for useful comments and suggestions.

REFERENCES

Ammann, C. 1996. Climate Change in den trockenen Anden: aktuelle Niederschlagsmuster. *Geogr. Bernesia* G46, 81–127.

Blatter, H., M. Funk and A. Ohmura. 1984. Atlas of solar climate. *Zürcher Geogr. Schr.* 10.

Budd, W. 1969. The dynamics of ice masses. *ANARE Sci. Rep., Ser. A (IV). Glaciol.* 108.

Clayton, J. D. and C. M. Clapperton. 1997. Broad synchrony of a late-glacial glacier advance and the highstand of paleolake Tauca in the Bolivian Altiplano. *J. Quat. Sci.*, **12** (3), 169–182.

Graf, K. 1991. Ein Modell zur eiszeitlichen und heutigen Vergletscherung in der bolivianischen Westkordillere. *Bamberger Geogr. Schr.* 11, 139–154.

Grosjean, M. 1994. Palaeohydrology of the Laguna Lejia (north Chilean Altiplano) and climatic implications for late-glacial times. *Palaeogeogr., Palaeoclimatol., Palaeoecol.*, **109**, 89–100.

Grosjean, M., M. Geyh, B. Messerli and U. Schotterer. 1995. Late-glacial and early Holocene lake sediments, groundwater formation and climate in the Atacama Altiplano. *J. Paleolimnol.*, **14**, 341–352.

Grosjean, M. *and 8 others*. 1996. Klimaforschung am Llullaillaco (Nordchile) — zwischen Pollenkörnern und globaler Zirkulation. *Jahrb. Geogr. Ges. Bern* 59, 111–121.

Grosjean, M., M. Geyh, B. Messerli, H. Schreier and H. Veit. 1998. A late-Holocene (<2600 BP) glacial advance in the south-central Andes (29° S), northern Chile. *Holocene*, **8** (4), 473–479.

Hastenrath, S. L. 1967. Observations on the snow line in the Peruvian Andes. *J. Glaciol.*, **6** (46), 541–550.

Hastenrath, S. L. 1971. On the Pleistocene snow-line depression in the arid regions of the South American Andes. *J. Glaciol.*, **10** (59), 255–267.

Hastenrath, S. and J. Kutzbach. 1985. Late Pleistocene climate and water budget of the South American Altiplano. *Quat. Res.*, **24** (3), 249–256.

Jenny, B. and K. Kammer. 1996. Climate Change in den trockenen Anden: jungquartäre Vergletscherung. *Geogr. Bernesia* G46, 1–80.

Kaser, G. 1996. Gletscher in den Tropen — ein Beitrag zur Geographie der tropischen Hochgebirge. (Habilitationsschrift, Universität Innsbruck.)

Kaser, G. and C. Georges. 1999. On the mass balance of low latitude glaciers with particular consideration of the Peruvian Cordillera Blanca. *Geogr. Ann.*, **81A** (4), 643–651.

Kaser, G., S. Hastenrath and A. Ames. 1996. Mass balance profiles on tropical glaciers. *Z. Gletscherkd. Glazialgeol.*, **32**, Part 2, 75–81.

Kessler, A. 1985. Zur Rekonstruktion von spätglazialem Klima und Wasserhaushalt auf dem peruanisch–bolivianischen Altiplano. *Z. Gletscherkd. Glazialgeol.*, **21**, 107–114.

Kessler, A. 1991. Zur Klimaentwicklung auf dem Altiplano seit dem letzten Pluvial. *Freibg. Geogr. Hefte* 32, 141–148.

Klein, A. G., G. O. Seltzer and B. L. Isacks. 1999. Modern and last local glacial maximum snowlines in the central Andes of Peru, Bolivia and northern Chile. *Quat. Sci. Rev.*, **18**, 63–84.

Kull, C. 1999. Modellierung paläoklimatischer Verhältnisse basierend auf der jungpleistozänen Vergletscherung in Nordchile — ein Fallbeispiel aus den Nordchilenischen Anden. *Z. Gletscherkd. Glazialgeol.*, **35** (1), 35–63.

Markgraf, V. 1993. Climatic history of central and South America since 18,000 yr B.P.: comparison of pollen records and model simulations. *In* Wright, H. E., Jr, *ed. Global climates since the Last Glacial Maximum*. Minneapolis, MN, University of Minnesota Press, 357–385.

Messerli, B. 1973. Problems of vertical and horizontal arrangement in the high mountains of the extreme arid zone (central Sahara). *Arct. Alp. Res.*, **5** (3), Part 2, A139–A147.

Messerli, B. *and 6 others*. 1996. Current precipitation, late Pleistocene snow line and lake level changes in the Atacama Altiplano (18° S–28°/29° S). *Bamberger Geogr. Schr.* 15, 17–35.

Oerlemans, J. 1997. A flowline model for Nigardsbreen, Norway: projection of future glacier length based on dynamic calibration with the historic record. *Ann. Glaciol.*, **24**, 382–389.

Paterson, W. S. B. 1994. *The physics of glaciers. Third edition*. Oxford, etc., Elsevier.

Seltzer, G. O. 1992. Late Quaternary glaciation of the Cordillera Real, Bolivia. *J. Quat. Sci.*, **7**, 87–98.

Seltzer, G. O. 1993. Late Quaternary glaciation as a proxy for climate change in the central Andes. *Mt. Res. Dev.*, **13** (2), 129–138.

Servant, M. *and 6 others*. 1993. Tropical forest changes during the Late Quaternary in African and South American lowlands. *Global and Planetary Change*, **7**, 25–40.

Sicart, J. E. *and 6 others*. 1998. *Mesures météorologiques, hydrologiques et glaciologiques sur le glacier du Zongo, année hydrologique 1996–97*. La Paz, ORSTOM. (Informe 57.)

Sylvestre, F., M. Servant, S. Servant-Vildary, C. Causse, M. Fournier and J.-P. Ybert. 1999. Lake-level chronology on the southern Bolivian Altiplano (18°–23° S) during late-glacial time and the Early Holocene. *Quat. Res.*, **51** (1), 54–66.

Thompson, L. G. *and 7 others*. 1995. Late glacial stage and Holocene tropical ice core records from Huascarán, Peru. *Science*, **269** (5220), 46–50.

Thompson, L. G. *and 11 others*. 1998. A 25,000-year tropical climate history from Bolivian ice cores. *Science*, **282** (5395), 1858–1864.

Vuille, M. 1996. Zur raumzeitlichen Dynamik von Schneefall und Ausaperung im Bereich des südlichen Altiplano, Südamerika. *Geogr. Bernesia* G45, 1–118.

Vuille, M. and C. Ammann. 1997. Regional snowfall patterns in the high, arid Andes (South America). *Climatic Change*, **36**, 413–423.

Wagnon, P., P. Ribstein, B. Francou and B. Pouyaud. 1999. Annual cycle of the energy balance of Zongo Glacier, Cordillera Real, Bolivia. *J. Geophys. Res.*, **104** (D4), 3907–3923.

MS received 5 January 2000 and accepted in revised form 12 July 2000